*Janusz M. Pawlikowski, Ewa Majchrowska and Piotr Becla**

Quantum Efficiency of PV-$Cd_xHg_{1-x}Te$ Detectors**

Photovoltaic p-n junction detectors made of epitaxial $Cd_xHg_{1-x}Te$ layers have been obtained with quantum efficiences up to 70%, at peak of photosensitivity, and at 77 K. The nature of PV-effect in these detectors especially the high values of quantum efficiency and their increase at greater energy of i.r. radiation have been discussed.

1. Introduction

Infrared detectors, especially those for the 8–14 μm atmospheric window, have been studied intensely over the recent years (see e.g. [1]). A few papers dealing with quantum efficiency of p-n junction of PV-$Cd_xHg_{1-x}Te$ detectors have been published recently (cf. [2–4]). The typical values of quantum efficiency obtained in these papers were below 50%, (usually about 10–15%), exceptionally about 65% in paper [4]. However, this high values were obtained only in waverange 1–3 μm.

In our previous papers [5, 6] we reported the technology and some electrical and photoelectrical properties of infrared PV detectors made of $Cd_xHg_{1-x}Te$ single crystals, and epitaxial $Cd_xHg_{1-x}Te$ layer, respectively, with the molar composition x ranging between 0.1 and 1. In this paper we present some results of the high-quantum efficiency detectors measurements and the discussion of the nature of the PV-effect in our detectors.

2. Results and discussion

A convenient method allowing to determine the quantum efficiency η is to measure the short-circuit current flow through the p-n junction (see e.g. [7]). If the radiation is absorbed within the junction and the lifetime of carriers generated is longer than the duration of the processes leading to their generation, then the value of short-circuit current density divided by electronic charge is equal to the number of carrier pairs created by photon absorption per second per unit area of the p-n junction cross-section. Therefore another method may be used by employing photovoltaic response measurements. The latter effect is also proportional to the number of free electron-hole pairs. However this course of action is hardly applicable for our samples at room temperature (and higher), because at this temperature it is difficult to obtain p-n junction with satisfactory rectifying properties — see [5]. Therefore the above mentioned method was succesfully used at 77 K.

In the photovoltaic mode the spectral dependence of the quantum efficiency η may be defined by the formula

$$S_\lambda = \eta(1-R_s)f, \tag{1}$$

where S_λ is a sensitivity of photoresponse in V/W, R_s is a reflection coefficient of the surface illuminated, and f is a factor, being function, in general, the physical phenomen in p-n junction and their properties, particularly of the absorption coefficient, lifetime of carriers generated and surface recombination velocity. The depth of the p-n junction position and the thicknes of the n- or p-type layer above the junction, as well as the presence of traping centers exert also influence on the spectral dependence of f-factor.

Very useful method for obtaining the spectral dependence of η is a simultaneous measurement of photoelectrical and electrical parameters (i.e. value of the both S_λ and differential resistivity of junction R_d [8]). Thus η can be written in the following form (for various wa-

* Institute of Physics, Wrocław Technical University 50-370 Wrocław, Wybrzeże Wyspiańskiego 27, Poland

** Work partially sponsored by Institute of Physics, Polish Academy of Science (Warsaw) and Wrocław Technical University under contract 60/75.

velength λ)

$$\eta_\lambda = S_\lambda \frac{hc}{e\lambda} R_d^{-1}, \qquad (2)$$

where h, c, and e are Planck constant, light velocity in vacuum and electron charge, respectively. Both the S_λ and R_d measurements have been described in our previous papers [5, 6]. Experimental setup used in measurements of spectral photoresponses is presented in Fig. 1.

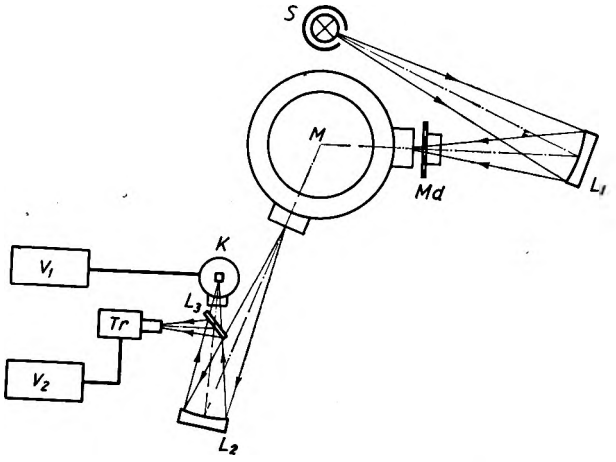

Fig. 1. Block diagram of the experimental setup used in the spectral measurement of detectors
M – monochromator SPM-1 (with NaCl prism), S – light source (SiC, 1500 K), L_1, L_2 – mirrors, M_d – chopper (10 Hz), L_3 – light-splitter (KRS-5 plate), K – cryostat with detector measured, T_r – thermocouple (VTh 5/7), $V_{1,2}$ – nanovoltmeters (Unipan 233)

Fig. 2 represents the spectral distribution of quantum efficiency at 77 K, obtained from eq. (2) for four typical detectors (for four different cutoffs of wavelength).

It has been cleary shown in Fig. 2, that two types of η vs wavelength plots were observed. First type has the relatively low (near absorption edge) and slowly-varying values of η up to wavelength with the energy about 0.5–0.7 eV. Second type has a high and narrow peak of η from 40 % up to 70 %; both types of η (λ) plots have been obtained for detectors without an antireflaction coating of detector surface. The η value equal to 70 % is a limiting value in this case for $Cd_xHg_{1-x}Te$ which has a reflection coefficient of about 30 % in 1–12 μm wavelength range [2, 9]. The second type has also the increasing values of η for energy about 0.5–0.7 eV. Two types of η (λ) plots have been shown more distinctly in Fig. 3, for the same cutoff of long-wavelength. The value of quantum efficiency near

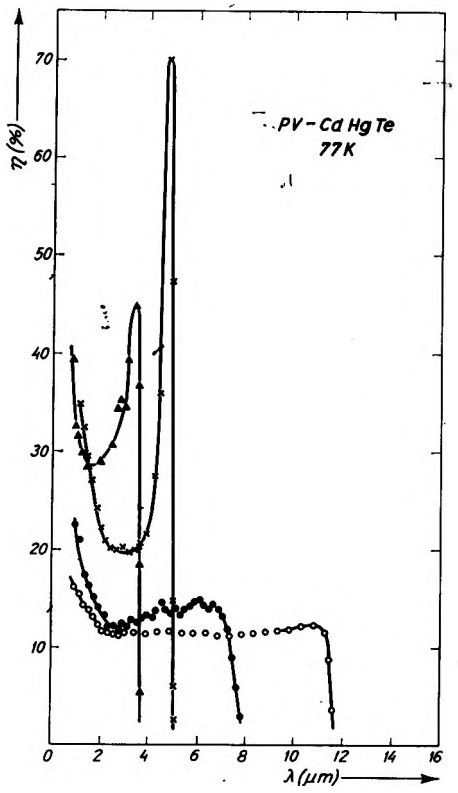

Fig. 2. Spectral dependence of quantum efficiency η for typicaly PV $Cd_xHg_{1-x}Te$ detectors

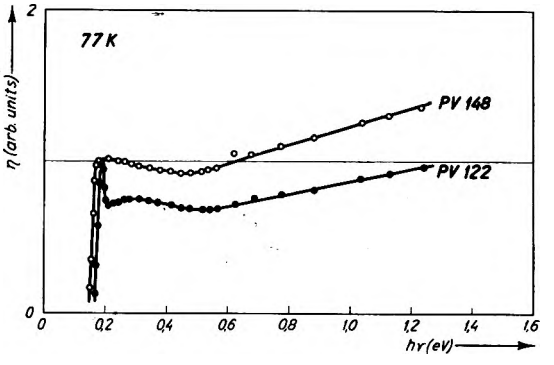

Fig. 3. η vs. $h\nu$ plot for two detectors at the same absorption edge

absorption edge has been assumed for convenience as equal to unity.

The very high selectivity PV detectors with a narrow peak of photoresponse and high quantum efficiency have been firstly obtained in our laboratory. The narrow and high-value peak of η may be explained with the help of the p-n junction S.E.L.D. (schematic energy level diagram) which was made on the basis of the electrical parameters of both n- and p-type regions. This diagram has been firstly presented in paper [10]. Such an S.E.L.D. for PV-Cd_xHg_{1-x} Te detector with molar composition near 0.3 for p-n junction

is shown in Fig. 4. The p-n junction is diffuse, due to the performed technology, i.e. Hg doping from vapour phase [11]. It may be easily seen (Fig. 4) that due to high concentration of donor impurities within the examined range

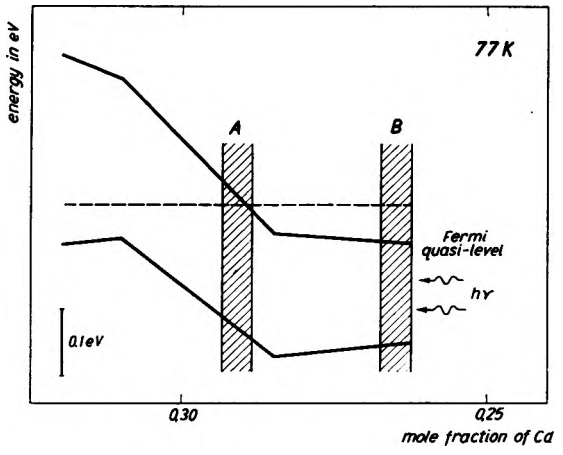

Fig. 4. Schematic energy band diagram of a graded-gap $Cd_xHg_{1-x}Te$ layer with diffusion p-n junction

of x, the Fermi level lies high in the conductivity band. A distinct Burstein-Moss effect [12,13] becomes evident for the radiation incident on the side with a smaller energy gap (for the mercury-rich back side). Then, the effective energy gap (including Burstein-Moss effect) on the B-space (see Fig. 4) is higher than on the A-space (e.g. from the diagram presented in Fig. 4. $E_g(A) - 0.20$ eV and $E_g(B) = 0.21$ eV, respectively). Hence the radiation incident on the region included within A–B and B will not be absorbed if $h\nu < E_g(A)$.

If the p-n junction is shallow, i.e. the distance d between A and B spaces fulfills the inequality $d < L_D$ (L_D denotes the diffusion length of carriers generated optically being equal to a few μm [14]) and surface recombination velocity is negligible, then the quantum efficiency of the PV-effect will depend mainly on the absorption coefficient within the junction region and achieve slowly-varying values within a relatively wide waverange, limited exclusively by the value of reflection coefficient (i.e. f-factor in eq. (1) is equal to constant, because each incident energy except for $h\nu < E_g(A)$, creates the free-carrier pairs within the whole space, if the lifetime of carriers generated is longer than the duration of the process of their diffusion to p-n junction).

If, however, the p-n junction is deep, i.e. $d \gg L_D$, then a high quantum efficiency (a large photoresponse) of PV-effect will be obtained when the radiation is absorbed in the A-space only, i. e. for $h\nu \cong E_g(A)$ only. For $h\nu > E_g(A)$ both the high light absorption and carrier generation regions shift toward the B-space, so only a small number of carriers can diffuse into the junction region. Consequently, the voltage of the PV-effect drops remarkably.

It has been noted, that in our typically epitaxial $Cd_xHg_{1-x}Te$ layer the distance between the molar compositions $x = 0.25$ and $x = 0.30$ is equal to about 70 μm (see e.g. [9]), i.e. distance between A and B spaces may be equal to about 40 μm. It is cleary observed, that this value is about four times higher than the diffusion length of carriers for these molar compositions [14].

After consecutive polishing and etching of the detectors surface was can to obtain the transition from high-selectivity detectors to ones with slowly-varying values of quantum efficiency.

The second effect i.e. the increasing η-values for greater energy of i.r. radiation which is shown in Figs 1,2, may be explained with the help of the model of phononless collision processes which can produce an additional electron-hole pair and has been widely discussed in paper [15]. From the ten probable types of two-stage ionization processes considered in [15], two processes schematically shown in Fig. 5 are most probable (see also [2, 7]). If the absorbed energy $h\nu$ of photons is greater than the energy gap E_g, the excess energy $h\nu - E_g$ is divided between the carriers generated, and two types of processes have to be considered: processes which do not change the number of free-carrier pairs, and processes which do change this number. In the second case the creation of additional carrier pairs by impact ionization will be shown to be the most important process. It can be also shown that the probability of recombination is much lower than the probability of impact ionization in the temperature range in which the spectral dependence of the quantum efficiency has been usually measured, so that the recombination process may be neglected.

The detailed form of the η vs. $h\nu$ dependence is determined both by the primary absorption process and by the secondary process including the electron-phonon interaction and impact ionization — as is shown in Fig. 5. During the primary absorption electrons from

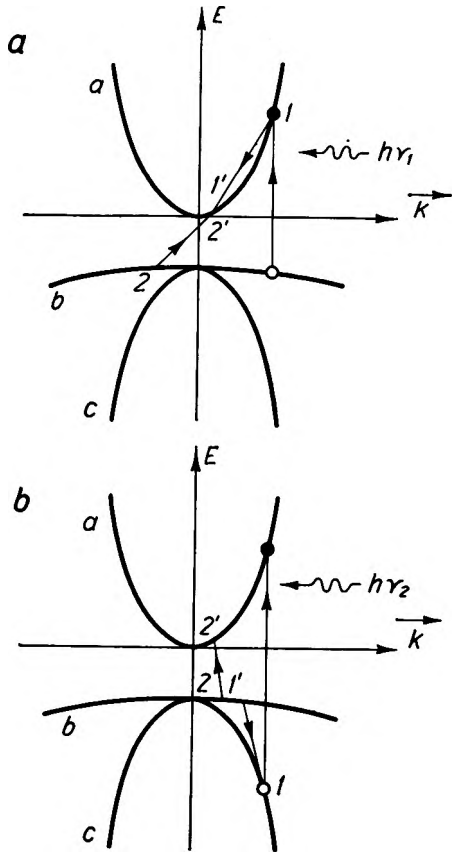

Fig. 5. Schematic level diagram presented two types of phononless collision processes which can produce and additional electron-hole pair

both the heavy hole band and the light hole band are excited into the conduction band. If electrons are excited from the heavy hole band (Fig. 5a) most of the excess energy $h\nu - E_g$ passes chiefly to electrons in conduction band (because of a large difference between the effective masses of both bands, greater than two order of magnitude). As long as the energies of these electrons are lower than a limiting value $h\nu_1$, the electron-phonon interaction is mainly dissipation process. For higher energies $h\nu$ the impact ionization takes place — — this process is connected with the first break* of η ($h\nu$) plot which was faintly emphasized in the majority of our detectors. If electrons are excited from light hole band (Fig. 5b) the excess energy $h\nu - E_g$ is passed almost equally to both electrons and holes. For photon energies $h\nu$ increasing up to second limiting value $h\nu = h\nu_2$ the impact ionization will also take place — this process is connected with the second break* of $\eta(h\nu)$ plot which was strongly emphasized in all the our detectors. The energies of both first and second breaks are shown in Table. In this table the theoretically calculated $h\nu_1$ and $h\nu_2$ values are also shown.

Detectors number	$h\nu_1$ (eV)		$h\nu_2$ (eV)	
	exper.	calculated	exper.	calculated
PV-122	0.22	0.34	0.49	0.49
PV-148	0.25	0.31	0.46	0.46
PV-115	0.43	0.40	0.73	0.69
PV-113	0.50	0.50	≅0.6	0.73

The $h\nu_1$ and $h\nu_2$ energy breaks (experimental and theoretical values, respectively).

They were estimated from simple equations (for parabolic bands) [15], describing the first impact ionization mechanism (Fig. 5a):

$$h\nu_1 - E_g = E_g\left(1 + \frac{2m_e^*}{m_{hh}^*}\right), \tag{3}$$

and the second one (Fig. 5b):

$$h\nu_2 - E_g = E_g\left(2 + \frac{m_{hl}^*}{m_{hh}^*}\right). \tag{4}$$

In eqs (3) and (4) m_e^*, m_{hl}^* and m_{hh}^* denote the effective masses of electron, light hole, and heavy hole, respectively. It has been assumed that $m_e^* = m_{hl}^*$ and their values have been taken from [16] for the respective molar composition x of $Cd_xHg_{1-x}Te$. The effective mass of heavy hole $m_{hh}^* = 0.55m_0$ for all compositions [17].

The satisfactory agreement between experiment and computed values has been obtained, taking into consideration the simplifying assumption referring mainly to the curvature of energy bands. The absence of first break of $\eta(h\nu)$ plots in the majority of our measured samples (stated also in [2]) cannot be satisfactorily explained and requires the additional measurements.

3. Final conclusions

The quantum efficiency η of p-n junction photovoltaic $Cd_xHg_{1-x}Te$ detectors has been measured and two phenomena have been obtained:

* It is easily seen that the electrons generated from heavy hole band rather will be the first to have the necessary energy (for impact ionization) than the electrons from light hole band.

— narrow and high-value peak of spectral dependence of η. This effect can be explained by schematic energy level diagram of p-n junction in which the distance between the junctions plane and detectors surface has a different value, in particular, greater or smaller than the diffusion length of carriers generated by photons.

— increase of η at photons energy greater than absorption edge. This effect can be explained by two simple models of phononless collision processes which have been described earlier in the papers cited.

Квантовый выход фотогальванических детекторов $Cd_xHg_{1-x}Te$

Квантовый выход детекторов с фотогальваническими переходами p—n, изготовленных из слоев $Cd_xHg_{1-x}Te$, составил 70% при пиковой светочувствительности и температуре 77 K. Обсужден вентильный характер фотоэффекта в парных детекторах со специальным учетом высоких значений квантового выхода и их роста с увеличением энергии инфракрасного излучения.

References

[1] Long D. and Schmit J. L., [in]: *Semiconductors and Semimetals*, ed. R. K. Willardson and A. C. Beer, Academic Press, New York and London, 1970, vol. V, p. 175.

[2] Ayache J. C. and Marfaing Y., Compt. Rend. Acad. Sci. Paris, **265**, 8363 (1967).

[3] Verie C. and Sirieix M., IEEE Quant. Electron. **QE-8**, 180 (1972).

[4] Soderman D. A. and Pinkston W. H. Appl. Optics **11**, 2162 (1972).

[5] Pawlikowski J. M. and Becla P., Infrared Phys. **15**, 331 (1975).

[6] Becla P. and Pawlikowski J. M., Infrared Phys. **16**, 475 (1976).

[7] Antončik E. and Tauc J., [in:] *Semiconductors and Semimetals*, ed. R. K. Willardson and A. C. Beer, Academic Press, New York and London 1966, Vol. II, p. 245.

[8] Long D., Infrared Phys. **12**, 115 (1972).

[9] Pawlikowski J. M., Becla P. and Dudziak E., Optica Appl. **6**, 3 (1976).

[10] Pawlikowski J. M., Infrared Phys. **17** (1977), in press.

[11] Becla P. and Pawlikowski J. M., Prace IF PWr **2**, 53 (1976).

[12] Burstein E., Phys. Rev. **93**, 632 (1954).

[13] Moss T. S., Proc. Phys. Soc. Lond. **67**, 30 (1954).

[14] Cohen-Solal G., Marfaing Y. and Kamadjiev P., Proc. Internat. Conf. Phys. II-VI Semiconductor Compounds, Providence, New York 1967, p. 1304.

[15] Beattie A. R., J. Phys. Chem. Solids. **23**, 1049 (1962).

[16] Stankiewicz J. and Giriat W., Prace ITE **2**, 61 (1971).

[17] Schmit J. L., J. Appl. Phys. **41**, 2876 (1971).

Received, March 18, 1976